Journal of Controlled Release 256 (2017) 193–202

Contents lists available at ScienceDirect

Journal of Controlled Release

journal homepage: www.elsevier.com/locate/jconrel

Mechanism-based selection of stabilization strategy for amorphous formulations: Insights into crystallization pathways

Khadijah Edueng[a,b], Denny Mahlin[a], Per Larsson[a], Christel A.S. Bergström[a,*]

[a] Department of Pharmacy, Uppsala University, Uppsala Biomedical Centre, P.O Box 580, SE-75123 Uppsala, Sweden
[b] Kulliyyah of Pharmacy, International Islamic University Malaysia, Jalan Istana, 25200 Bandar Indera Mahkota, Kuantan, Pahang, Malaysia

ARTICLE INFO

Keywords:
Amorphous
Crystallization
Solid-state
Dissolution
Stabilization
Polymer
Supersaturation

ABSTRACT

We developed a step-by-step experimental protocol using differential scanning calorimetry (DSC), dynamic vapour sorption (DVS), polarized light microscopy (PLM) and a small-scale dissolution apparatus (μDISS Profiler) to investigate the mechanism (solid-to-solid or solution-mediated) by which crystallization of amorphous drugs occurs upon dissolution. This protocol then guided how to stabilize the amorphous formulation. Indapamide, metolazone, glibenclamide and glipizide were selected as model drugs and HPMC (Pharmacoat 606) and PVP (K30) as stabilizing polymers. Spray-dried amorphous indapamide, metolazone and glibenclamide crystallized via solution-mediated nucleation while glipizide suffered from solid-to-solid crystallization. The addition of 0.001%–0.01% (w/v) HPMC into the dissolution medium successfully prevented the crystallization of supersaturated solutions of indapamide and metolazone whereas it only reduced the crystallization rate for glibenclamide. Amorphous solid dispersion (ASD) formulation of glipizide and PVP K30, at a ratio of 50:50% (w/w) reduced but did not completely eliminate the solid-to-solid crystallization of glipizide even though the overall dissolution rate was enhanced both in the absence and presence of HPMC. Raman spectroscopy indicated the formation of a glipizide polymorph in the dissolution medium with higher solubility than the stable polymorph. As a complementary technique, molecular dynamics (MD) simulations of indapamide and glibenclamide with HPMC was performed. It was revealed that hydrogen bonding patterns of the two drugs with HPMC differed significantly, suggesting that hydrogen bonding may play a role in the greater stabilizing effect on supersaturation of indapamide, compared to glibenclamide.

1. Introduction

Limited aqueous solubility is one of the major factors associated with poor oral bioavailability and erratic effects *in vivo* [1]. A formulation route that has received much attention is the production of poorly soluble drugs in their amorphous form, mainly by formulating them as amorphous solid dispersion (ASD) with one or more excipient (s). An increasing number of studies focus on understanding the formulation systems with regard to physicochemical properties of the components, i.e., the active pharmaceutical ingredients, (APIs) and excipients; molecular interactions between these components; and processes during the dissolution *in vitro* and *in vivo* [1–4]. Better knowledge on formulations has set a strong platform for ASD to be regarded as a viable strategy for overcoming solubility problems. This was proven by an increasing number of pharmaceutical products based on ASD technologies that have gained approval from the FDA within the past years [5].

However, amorphous systems are associated with instability problems. Although the instability is thermodynamically driven by the free-energy difference between the amorphous and crystalline states, the propensity for transformation from the former to the latter is strongly linked to kinetic factors such as nucleation probability and molecular mobility in the amorphous state. The transformation leads to the loss of the solubility advantage conferred by amorphization [6]. Crystallization of amorphous system can occur in the solid-state (e.g. during processing, handling and storage) and during dissolution. Upon dissolution, the crystallization of an amorphous system occurs through either solid-to-solid or solution-mediated transformation [6,7]. In solid-to-solid transformation, the increase in temperature or water sorption increases the molecular mobility of the amorphous system which may lead to an increase in the crystallization rate [6]. In contrast solution-mediated crystallization requires a supersaturated solution [6–9]. Both solid-to-solid and solution-mediated transformations start with nucleation in which stable nuclei are formed, followed by crystal growth

* Corresponding author at: Department of Pharmacy, Uppsala University, Box 580, SE-751 23 Uppsala, Sweden.
E-mail addresses: khadijah.edueng@farmaci.uu.se (K. Edueng), denny.mahlin@farmaci.uu.se (D. Mahlin), per.larsson@farmaci.uu.se (P. Larsson), christel.bergstrom@farmaci.uu.se (C.A.S. Bergström).

http://dx.doi.org/10.1016/j.jconrel.2017.04.015
Received 17 January 2017; Received in revised form 9 April 2017; Accepted 10 April 2017
Available online 12 April 2017

[6–8]. The formation of stable nuclei is the rate-limiting step, as it requires overcoming a nucleation barrier, but subsequent crystal growth can be rapid, and is accelerated by increasing temperature [8].

Theoretically, the driving force for nucleation depends on the free concentration of the drug available in the medium and the level of supersaturation controls the rate of crystal growth. The higher the free concentration of drug, the greater the probability for the nucleation to take place [10]. Crystallization by either mechanism (solid-to-solid and solution-mediated transformation) may be reduced, or even inhibited, by the addition of excipients (usually polymers).

The crystallization behaviour of amorphous formulations in the solid and dissolved states can be studied by differential scanning calorimetry (DSC), thermogravimetric analysis (TGA), dynamic vapour sorption (DVS), polarized light microscopy (PLM), powder x-ray diffraction (XRPD), Raman spectroscopy, and dissolution assays [7,8,11–13]. Few years ago, Alonzo and co-workers introduced the use of different experimental techniques including XRPD, microscopy, Raman spectroscopy and small-scale dissolution apparatus to study the behaviour of amorphous systems during dissolution [7] and the effect of polymers on their dissolution and precipitation behaviour [14]. In a more recent study, Mah *et al.* reported the superiority of DSC compared to Raman spectroscopy in predicting the physical stability and dissolution performance of milled amorphous glibenclamide [15]. Despite the extensive use of these techniques, they have not been combined as a standardized experimental protocol especially to predict crystallization during dissolution and guide the design of amorphous formulations. The addition and selection of polymer(s) to stabilize amorphous formulations is often based on trial-and-error experiments, usually without any sound scientific rationales [16–18]. Typically, the performance of amorphous formulations is evaluated by analyzing the dissolution profile in combination with investigations of the physical stability. The dissolution profile i.e., dissolution rate, degree of supersaturation and area under the dissolution curve, are affected by recrystallization. Thus, dissolution can be compromised if the amorphous drug recrystallizes. In this study, we developed a standardized experimental method to reveal the crystallization mechanisms that impact the dissolution profile of a particular amorphous drug. A combination of small-scale solid characterization methods and an *in vitro* dissolution assay under non-sink condition were used to differentiate between solid-to-solid and solution-mediated crystallization occurring during dissolution. The molecular interactions between the drug and polymer were further studied by molecular dynamic (MD) simulations to understand the specific mechanisms by which the polymer inhibits crystallization of supersaturated system.

2. Materials and methods

2.1. Materials

Glibenclamide, glipizide, PVP K30, sodium hydroxide (purity ≥ 98%), sodium phosphate (purity ≥ 99%), sodium chloride (purity ≥ 99%) and dimethyl sulfoxide (purity ≥ 99.9%) were purchased from Sigma-Aldrich (Germany). Indapamide was purchased from Tokyo Chemical Industry Co. Ltd., (Tokyo, Japan) and metolazone from APIChem (China). Hydroxypropylmethyl cellulose (HPMC) grade 606 was obtained from Shin Etsu (Tokyo, Japan). Acetone (purity ≥ 99.8%) was obtained from Merck (Germany) and ethanol (purity ≥ 99.7%) from Solveco (Sweden). Phosphorus pentoxide was purchased from VWR Chemicals (Leuven, Belgium). The chemical structures of the four model drugs are depicted in Fig. 1 and their physicochemical properties summarized in Table 1.

2.2. Methods

In this study, we employed different experimental techniques in a step-wise approach as shown in Fig. 2. The detailed protocol of each technique is explained below.

2.2.1. Preparation of amorphous drug and amorphous solid dispersion

The crystalline drugs were transformed to their amorphous form by spray drying using a Büchi Mini Spray Dryer B-290 (Switzerland). The spray-drying parameters used throughout the study were: inlet temperature (55 °C), aspiration rate (75%) and pump rate (4 mL/min). The solutions of pure drug for spray drying were prepared by dissolving the drug powder in 10:90% (w/w) acetone and ethanol. The amount of drug powder was kept at ≤ 75% of its solubility to diminish the risk of any non-dissolved, crystalline drug in the solvent mixture. The amorphous solid dispersion (ASD) solution for spray drying was prepared by dissolving the drug powder and PVP (K30) in the same solvent mixture of acetone and ethanol. The final weight ratio of the dissolved compounds was 50:50 (drug/PVP). The spray dried (SD) neat drugs and ASD were stored in a vacuumed desiccator containing phosphorus pentoxide until further analyses. The amorphous nature of spray dried SD drugs and ASD was confirmed by DSC and PLM immediately after spray drying and before proceeding with experiments and analyses for stored materials.

2.2.2. Solid state characterization

2.2.2.1. DSC. A DSC Q2000 Differential Scanning Calorimeter (TA Instrument Co., USA) was used to analyse the thermal behaviour of the unprocessed crystalline drugs, SD neat drugs, and ASD, before and after humidity exposure. Depending on the sensitivity required for the analyses, either standard DSC or modulated DSC was used. The DSC cell was calibrated with indium (melting temperature, T_m = 156.59 °C and heat of fusion, H_f = 28.57 J/g) and purged with 50 mL/min of nitrogen. Detailed protocols for the DSC and modulated DSC (MDSC) are provided below.

2.2.2.2. Conventional DSC. For unprocessed crystalline as well as for SD drugs, 1–5 mg of sample was weighed into an aluminium pan that was sealed with an aluminium lid containing pin holes. An initial heat-cool-heat cycle was used for SD samples (both neat drug and ASD) to remove residual solvent: the sample was first equilibrated at 0 °C, heated at 10 °C/min to 110 °C and held for 5 min, then cooled to 0 °C at 10 °C/min. For thermal analysis, the sample was then equilibrated at 0 °C, and thereafter heated at 10 °C/min to 30–50 °C above its melting point. From the resulting thermograms, the melting temperature (T_m) was determined for the unprocessed crystalline sample. The glass transition temperature (T_g), crystallization temperature (T_c) and melting temperature (T_m) were determined for SD neat amorphous drug and ASD samples. Onset values are reported.

2.2.2.3. MDSC. To determine some of the T_g values and to separate overlapping thermal events, increased sensitivity was needed and MDSC was therefore used. The sample was equilibrated at 0 °C, modulated at ± 0.5 °C every 60 s, and heated at 1 °C/min to a temperature 30–50 °C above its melting point. T_g was determined from the reversible heat flow signal.

2.2.2.4. Polarized light microscopy (PLM). Images of SD neat drugs and ASD were collected using an Olympus BX51 microscope (Tokyo, Japan) at three time points: (i) immediately after obtaining the spray dried material; (ii) 24 h post exposure in the DVS chamber (98% RH, see Section 2.2.3); and (iii) 4 h post dissolution at 37 °C (see Section 2.2.4). Samples were dispersed in olive oil for better image quality and clarity, except for the post dissolution samples. These were already dispersed in the dissolution media and therefore analyzed directly.

2.2.3. Exposure to high humidity

The solid-to-solid crystallization of the SD neat amorphous drugs and ASDs were investigated by DVS (DVS Advantage, Surface Measurement System Ltd., UK). Approximately 1.5–2.0 mg of samples

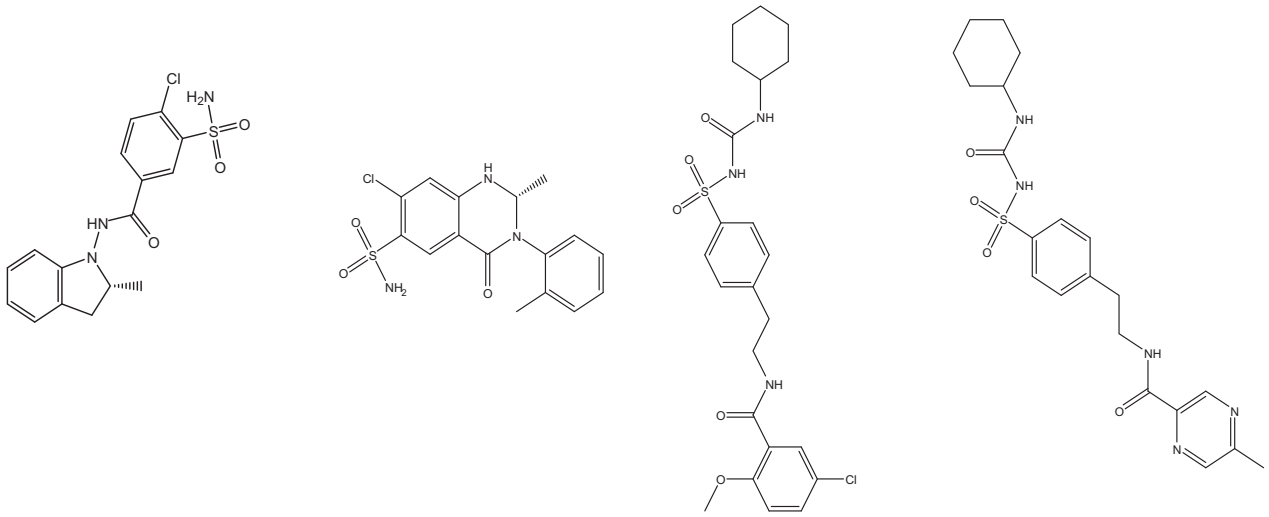

Fig. 1. Model compounds included in the study. From left to right: indapamide, metolazone, glibenclamide and glipizide.

Table 1
Physicochemical properties of model drugs.

Compound	Mw[a] (g/mol)	logP[a]	pKa[a]	T_m[b] (°C)	T_c[c] (°C)	T_g[c] (°C)	$S_{PhB6.5}$[d] (μg/mL)
Indapamide	365.8	2.9	8.8	165	nd	102	86.71 ± 2.9
Metolazone	365.8	4.1	9.7	268	203	117	47.80 ± 1.8
Glibenclamide	494.0	4.8	5.3	174	135	70	1.23 ± 0.5
Glipizide	445.5	1.9	5.9	207	95	59	11.66 ± 1.1

Not detected (nd).

[a] Molecular weight (MW), calculated logP (XLogP), acid dissociation constant (pKa) were extracted from the PubChem database (http://pubchem.ncbi.nlm.nih.gov/).

[b] In-house determination of melting point (T_m) from raw materials with DSC using a heating rate 10 °C/min.

[c] In-house determination of crystallization temperature (T_c) and glass transition temperature (T_g) from spray dried amorphous samples using DSC and a heating rate 10 °C/min.

[d] Equilibrium solubility (S) of crystalline drugs in phosphate buffer pH 6.5($PhB_{6.5}$) containing 0.029 M phosphate and 0.106 M NaCl measured with pION μDISS dissolution apparatus at 37 °C.

were weighed in DSC sample pans without lids and placed on the microbalance. The samples were initially pre-heated at temperatures 10–20 °C below their onset of T_g for about 1 h to remove any residual solvent from the samples. Thereafter, the samples were exposed to humidity (%RH) ramped from 0% to 98% RH within 2 min and kept at 98% and 25 °C for 24 h. After 24 h, the samples were removed and re-analyzed by DSC and PLM for changes in the solid state i.e., whether the drug had re-crystallized at this condition.

2.2.4. Dissolution studies under non-sink conditions

The dissolution studies of crystalline and SD amorphous drug under non-sink conditions were performed in a small-scale dissolution apparatus (μDISS Profiler, pION INC, USA). The instrument used in this study has three parallel dissolution vials, each with a UV probe. Probe tips with path length ranging between 5-mm and 20-mm were selected depending on the solubility of the drug. Phosphate buffer at pH 6.5 containing 0.029 M phosphate and 0.106 M NaCl ($PhB_{6.5}$) was used as the dissolution medium with or without HPMC at a concentration range of 0.001%–0.01% (w/v). All dissolution studies were performed in at least triplicate, at 37 °C, using a stirring rate of 100 rpm. The modified and down-scaled protocol recommended by Andersson *et al.* is briefly described below [19].

First, each UV probe was calibrated separately. The standard calibration curves were obtained by adding 4–15 μL aliquots of DMSO stock solutions to 3 mL of $PhB_{6.5}$ (37 °C), stirring at 800 rpm for 1 min, then collecting the UV-spectrum. The second derivative of the spectra at wavelengths specific to the samples was used to minimize particle scattering effects. Once the standard calibration curve was established, the dissolution studies were conducted by adding an excess amount of samples (10-fold higher than the equilibrium solubility in the $PhB_{6.5}$ used ($S_{PhB6.5}$; see Table 1)) to 3 mL of $PhB_{6.5}$ with or without HPMC at the concentrations mentioned above. The dissolution, and possible solution-mediated crystallization, was followed for 4 h to reflect the transit time of drug through the small intestine.

2.2.5. Precipitation behaviour by solvent shift

Studies on the precipitation behaviour by solvent shift were performed for glibenclamide since this was the only drug that did not maintain the supersaturation in presence of HPMC in the dissolution medium. A solution of glibenclamide in DMSO was added to 3 mL $PhB_{6.5}$ in a dissolution vial to produce a supersaturated solution with a concentration 10-fold higher than the equilibrium glibenclamide solubility. The final DMSO concentration in the vial was < 2% to minimize the influence of co-solvent on the resulting processes. The experiment was performed with the μDISS Profiler as described in Section 2.2.4.

2.2.6. Raman spectroscopy

To investigate the occurrence of polymorphism, the precipitate remaining after the dissolution of glipizide was investigated using an Rxn-2 Hybrid Raman Spectrometer (Kaiser Optical System Inc., Ann Arbor, MI) with a laser wavelength of 785 nm and laser power of 400 mW. Spectra were collected for the unprocessed glipizide and solid material of glipizide obtained after the dissolution study. A fiber-optic PhAT probe was used and the spectra were monitored in the range 100–1890 cm^{-1}.

2.2.7. Molecular dynamics (MD) simulations

Small-scale MD simulations were performed as a complementary method to study the effects of HPMC upon drug stability during dissolution of the drug. Indapamide and glibenclamide were selected as the model drugs for the simulations based on their different dissolution profiles and stability of supersaturation in the presence of HPMC. Indapamide represents the stable supersaturated system whereas glibenclamide represents the unstable supersaturated system.

The simulations were carried out using the Generalized Amber Forcefield (GAFF) [20] and Gromacs version 5 [21,22]. The initial charge derivation for indapamide, glibenclamide and HPMC monomer units was calculated from the electrostatic potentials (ESPs) at the HF/6-31G(d) level of theory, followed by fitting of the ESPs with the restrained electrostatic potential (RESP) method available through the

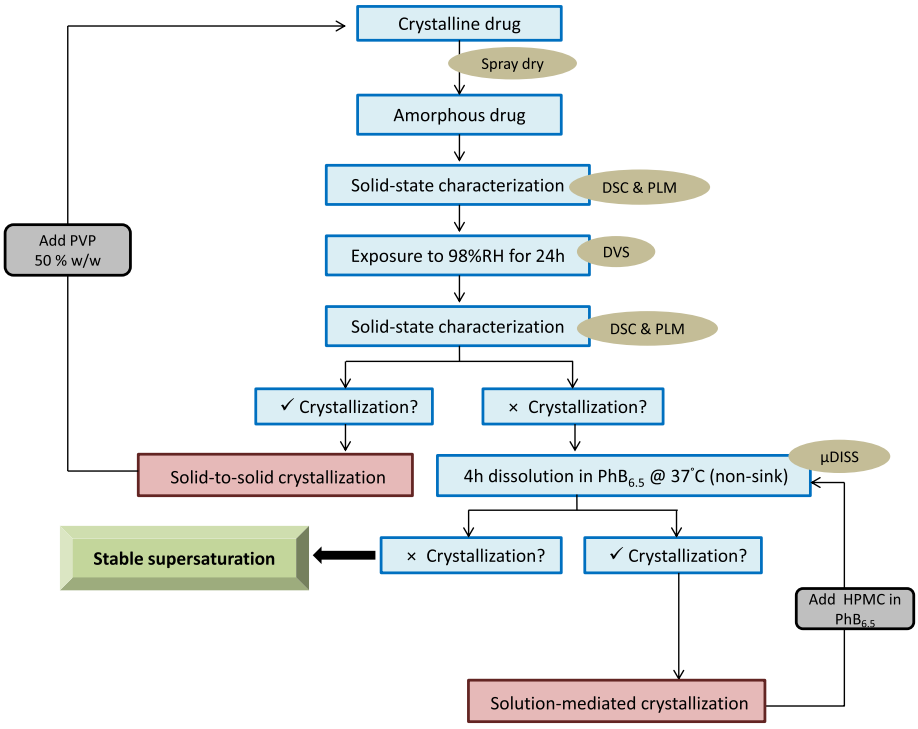

Fig. 2. Summary of the experimental protocol to select the stabilization strategy for amorphous formulation.

PyRED server [23]. All other GAFF interaction parameters in Gromacs format were obtained using the STaGE software [24].

To construct the polymer chains, a simple in-house python script was developed to repeatedly position HPMC monomer units on a regular grid with a suitable spacing (essentially the end-to-end distance of a monomer unit). This was followed by 500 steps of steepest descent energy minimization to relieve bad atom contacts and clashes and a short in-vacuo MD run to collapse the initially straight polymer chains. This was done individually for all polymer chains in the simulations, so as to randomize the polymers as much as possible. The commercial HPMC used in this study has an average molecular weight of approximately 35,600 Da. To make molecular simulation feasible, we used a shorter polymer chain (corresponding to around 10% of 35,600 Da). We also varied the amount of drug to more rigorously study the drug–polymer molecular interactions on a per–molecule level. The number of drug and HPMC molecules in the simulations was calculated based on the number of moles used in their respective dissolution experiment. Hence, the number of drug molecules is equivalent to 10-fold the equilibrium solubility in $PhB_{6.5}$ to create the supersaturation whereas the number of HPMC molecules corresponds to 0.01% w/v added in the $PhB_{6.5}$, and with the final number of drug molecules then adjusted to the shorter polymer length used in the simulations. Additional simulations with only drug molecules and water were also performed, again with varying numbers of the drug molecules. This resulted in a total of eight simulations (see Table 2). In all cases, the total water content was constant at 90% (w/w), and the length of each individual simulation was up to 100 ns. All initial assemblies with drugs and polymer molecules were constructed using Packmol [25], followed by the addition of water using the Gromacs gmx solvate utility. Steepest descent energy minimization for 5,000 steps was then performed, followed by equilibration of pressure and density and finally production runs at 298 K and 1 bar. During these runs, coordinates and velocities were saved every ns for subsequent analysis.

All simulations (equilibration and production) were performed using the verlet cut-off scheme. The time step was 2 fs, and system temperature and pressure were maintained by the velocity rescale thermostat [26] and Parrinello-Rahman barostat [27], respectively.

Table 2
Composition of the simulated assemblies.[a]

Drug	System (drug concentration)	HPMC presence	Drug molecules	Polymer chains	Water molecules
Indapamide	Low	Yes	41	10	30,040
	High	Yes	851	10	178,000
	Low(drug only)	No	41	0	7,500
	High (drug only)	No	851	0	155,661
Glibenclamide	Low	Yes	41	10	32,667
	High	Yes	851	10	232,739
	Low(drug only)	No	41	0	10,127
	High(drug only)	No	851	0	210,198

[a] The number of molecules in each system was calculated from the 10-fold measured equilibrium solubility of indapamide (851) and glibenclamide (41) in the dissolution medium, starting from a dissolution medium volume of 3 mL, and then adjusted to reflect the use of HPMC with a lower molecular weight (about 10% of 35,600 Da per polymer chain). To allow comparison of molecular interactions for these two drugs, additional simulations at the concentration of the 10-fold equilibrium solubility of indapamide for glibenclamide (i.e. 851 glibenclamide molecules, high) and that of glibenclamide for indapamide (41 molecules, low) as well as simulations of polymer-free systems were performed.

Electrostatic interactions were calculated using the Particle Mesh Ewald method [28] with a real-space cutoff of 1.0 nm. All covalent bonds involving hydrogens were constrained via the P-LINCS [29] algorithm. Van der Waals interactions also used a 1.0 nm cutoff, with long-range dispersion correction applied to both energy and pressure. Hydrogen bond analysis was performed using the gmx hbond utility in Gromacs 5. Snapshot images were produced using VMD [30].

3. Results

3.1. Exposure to high humidity

The DSC thermograms of the four model drugs are shown in Fig. 3. Spray-dried indapamide, metolazone, glibenclamide and glipizide

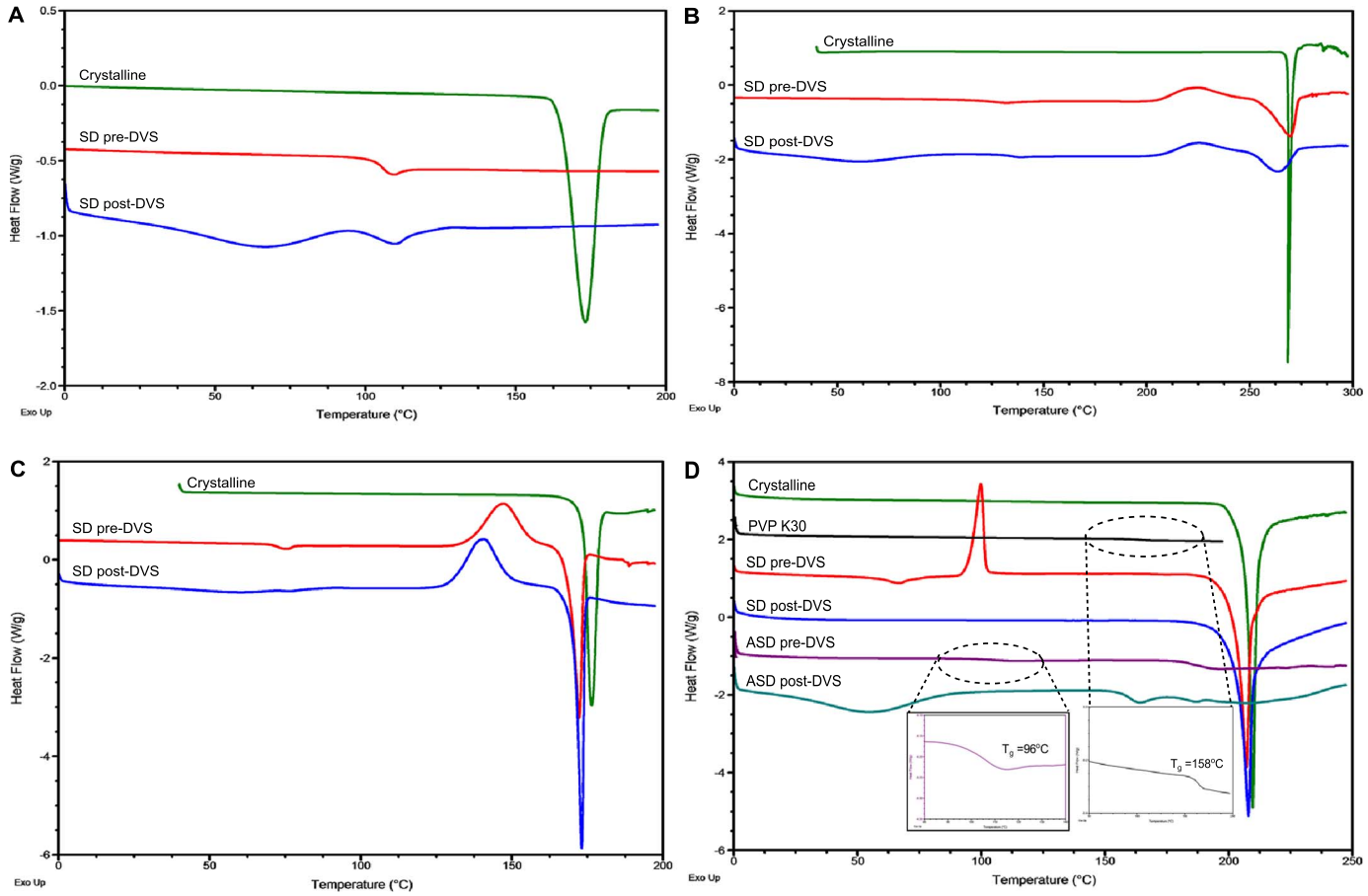

Fig. 3. DSC thermograms of (A) indapamide, (B) metolazone, (C) glibenclamide and (D) glipizide. Unprocessed crystalline (green), spray dried before humidity exposure (red), spray dried after humidity exposure (blue), ASD before humidity exposure (purple) and ASD after humidity exposure (cyan). For comparison, the thermogram of PVP K30 is shown (black).

showed T_g at 102 °C, 117 °C, 70 °C, and 59 °C, respectively. No changes in the thermal profiles were observed in the DSC thermograms of indapamide, metolazone and glibenclamide before (pre-DVS) and after (post-DVS) exposure to humidity, except for the appearance of water evaporation endotherms before and/or around the T_g in the post-DVS samples (see Fig. 3a–c). The T_g values broadened and shifted to a lower temperature range in the DSC thermograms, presumably as a consequence of water sorption during the exposure. There was no crystallinity observed in the PLM images of the post-DVS samples (see Supplementary 2a–c).

In contrast, glipizide showed significant crystallization during exposure to humidity, as evidenced by the disappearance of glass transition and the appearance of a melting peak in the DSC thermogram. Furthermore, in the PLM images crystal phase was observed as bright areas in cross-polarized light in the post-DVS sample (see Supplementary 2d). Due to the solid state instability of SD glipizide alone, the drug was spray dried with PVP in a 50:50% (w/w) ratio to form an ASD. A single T_g at 96 °C was detected in the DSC thermogram of the ASD indicating that glipizide and PVP were molecularly dispersed. The resulting ASD was then subjected to the same high humidity condition in DVS after which the DSC analyses were repeated. No obvious T_g could be detected in the DSC thermograms of the post-DVS samples (see Fig. 3d). Three small and broad endotherms were observed, the first being water de-sorption upon heating. However, the other two transitions occurring between 150 °C and 200 °C could not with certainty be identified as glass transition or melting events. MDSC was therefore performed on the ASD samples, pre- and post-DVS, and pure PVP. T_g was detected a few degrees higher than in the ordinary DSC analysis for ASD pre-DVS and pure PVP in the reversing heat signal (see Supplementary 1). The only clear events observed post-DVS is a glass transition just 10 °C below the T_g of the pure PVP. Furthermore, an endothermic event with peak value of 166 °C is observed in the reversed heat flow signal. It should be pointed out that this cannot be the relaxation peak commonly found at T_g, since that would only appear in the non-reversing signal. However, the PLM did not indicate any crystalline phase present after humidity exposure (see Supplementary 2d). Hence, the data is not straight forward to interpret but indicates that during the exposure to this high humidity the glipizide in the ASD has started to convert to another polymorph.

3.2. Dissolution of amorphous drugs and ASDs

Dissolution studies with HPMC were performed to investigate whether this polymer could reduce the solution-mediated crystallization and stabilize the supersaturated state. Fig. 4a shows the dissolution profile of indapamide. The maximum level of supersaturation (C_{ss}) of amorphous indapamide in pure $PhB_{6.5}$ was 102.2 ± 27.1 μg/mL, only 1.2 times higher than the equilibrium solubility of 86.7 ± 2.9 μg/mL. It reached its maximum concentration (C_{max}) within 15 min and thereafter decreased to reach the equilibrium (crystalline) solubility within the 4 h studied. The effect of pre-dissolved HPMC (0.001% and 0.01% (w/v)) in the $PhB_{6.5}$ on C_{ss} was therefore investigated. Even though a higher C_{ss} was achieved in the presence of low concentration of HPMC (189.9 μg/mL ± 40.1, vs. 102.2 ± 27.1 without), the indapamide began to crystallize already after 5 min and its concentration thereafter declined to the equilibrium solubility. The higher concentration of HPMC successfully inhibited crystallization and no precipitation was observed. The C_{ss} achieved was 525.5 ± 19.5 μg/mL, 6-fold higher than the equilibrium solubility, and this level was maintained during the course of the experiment. The changes in

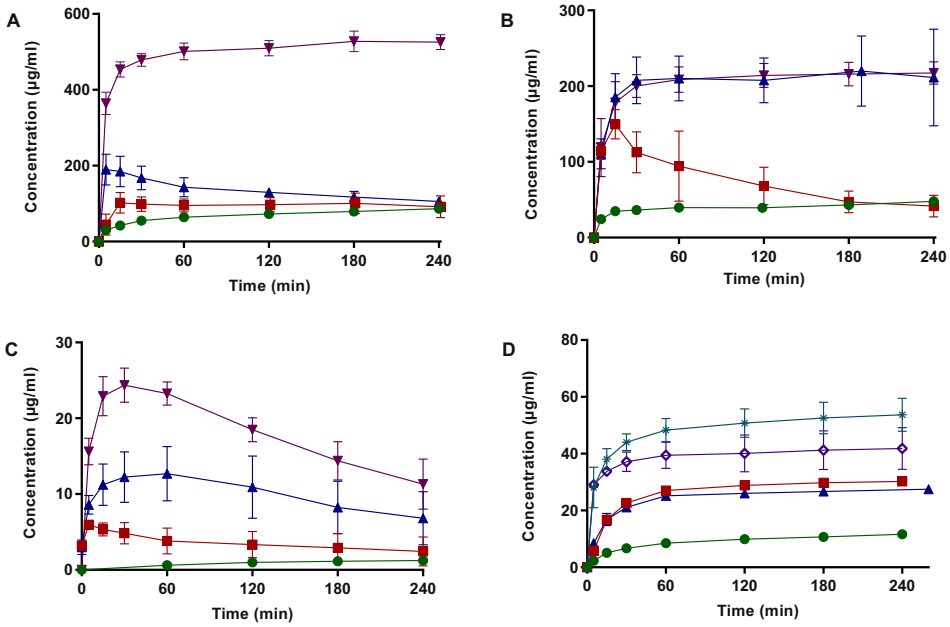

Fig. 4. Dissolution profiles of (A) indapamide, (B) metolazone, (C) glibenclamide and (D) glipizide at 37 °C under non-sink conditions. In every panel, represents the respective crystalline drug in pure $PhB_{6.5}$, represents amorphous drugs in pure $PhB_{6.5}$, represents amorphous drugs in$PhB_{6.5}$ + 0.001% (w/v) HPMC and represents amorphous drugs in $PhB_{6.5}$ + 0.01% (w/v) HPMC, represents ASD of glipizide: PVP K30 50:50% (w/w) in pure $PhB_{6.5}$ and represents ASD of glipizide:PVP K30 50:50% (w/w) in $PhB_{6.5}$ + 0.001% (w/v) HPMC. Each value represents the mean ± SD (n ≥ 3).

dissolution profiles were supported by PLM images which showed crystallinity in post-dissolution samples from pure $PhB_{6.5}$, and $PhB_{6.5}$ with 0.001% (w/v) HPMC, but not in samples containing 0.01% (w/v) HPMC (see Supplementary 4a).

Dissolution of different metolazone samples was also studied (Fig. 4b). In pure $PhB_{6.5}$, amorphous metolazone supersaturated at 149.6 ± 19.3 µg/mL within 15 min, but the level decreased to the equilibrium solubility (47.8 ± 1.8 µg/mL) during the time course of the experiment (4 h). With 0.001% (w/v) HPMC in the $PhB_{6.5}$, the metolazone reached a significantly higher C_{ss} (211.4 ± 63.7 µg/mL, 4.4-fold higher than the equilibrium solubility) and this concentration was maintained during the course of the experiment. Quite extensive crystal formation was visible in PLM images of post-dissolution sample from pure $PhB_{6.5}$ and interestingly, traces of crystallinity were also observed in samples extracted from $PhB_{6.5}$ with 0.001% (w/v) HPMC (see Supplementary 4b). Increasing the HPMC concentration to 0.01% (w/v) in the $PhB_{6.5}$ did not increase the level of metolazone supersaturation and crystallinity was also observed in the PLM images of post-dissolution samples from $PhB_{6.5}$ with 0.01% (w/v) HPMC presence (see Supplementary 4b).

The dissolution of amorphous glibenclamide in $PhB_{6.5}$ reached a C_{ss} of 6.0 ± 0.2 µg/mL in 5 min but decreased almost immediately and reached its equilibrium solubility. The addition of HPMC in the $PhB_{6.5}$ did not completely stabilize the supersaturation. With the addition of 0.001% (w/v) HPMC, a level of 12.7 ± 3.6 µg/mL was reached in 1 h whereas > 24.4 ± 2.3 µg/mL was reached within 30 min at 0.01% (w/v) HPMC before the crystallization dominated and the concentration slowly decreased. These observations were supported by the PLM images showing crystalline phase in all of the post-dissolution samples (see Supplementary 4c). The solvent shift experiment showed a similar concentration-time profile despite the higher C_{ss} (41.2 ± 4.3 µg/mL) achieved with 0.01% (w/v) HPMC (see Supplementary 3).

Glipizide showed a completely different dissolution profile than the other three model drugs (see Fig. 4d). The solubility of crystalline glipizide was 11.7 ± 1.1 µg/mL. Upon dissolution, the spray-dried neat glipizide reached a maximum concentration, C_{max}, at 30.2 ± 0.9 µg/mL after 4 h in the $PhB_{6.5}$. A similar trend was observed for dissolution in $PhB_{6.5}$ with 0.001% (w/v) HPMC added (C_{max} 27.5 ± 1.5 µg/mL). In both cases, the C_{max} was higher than that for the crystalline counterpart. The dissolution rate of the ASD (50:50% (w/w) glipizide:PVP K30) was higher than spray-dried neat glipizide both with and without 0.001% (w/v) HPMC, where the C_{max} were 53.7 ± 5.8 and 41.8 ± 7.3 µg/mL, respectively. This is 4–5 times higher than the equilibrium solubility. The PLM images of post-dissolution samples of spray-dried neat glipizide showed some crystallinity both with and without HPMC. However, there was no visible crystal formation in the post-dissolution samples of ASD, regardless of HPMC addition (see Supplementary 4d).

3.3. Raman spectroscopy

The Raman spectra of the unprocessed crystalline and the solid material of glipizide after the dissolution study are shown in Fig. 5. The spectrum of solid material collected after the dissolution study is clearly different in terms of peak positions and intensity compared to the spectrum of unprocessed glipizide, which suggests that another polymorph of glipizide had been formed.

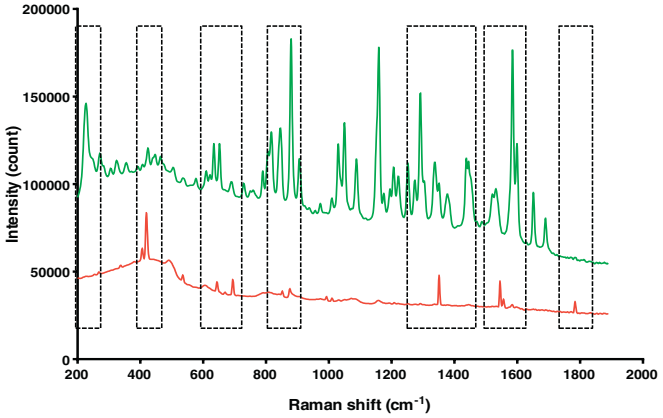

Fig. 5. Raman spectra of different glipizide samples: Unprocessed crystalline (green) and spray dried after dissolution (red). Highlighted regions indicate Raman shifts of the peaks.

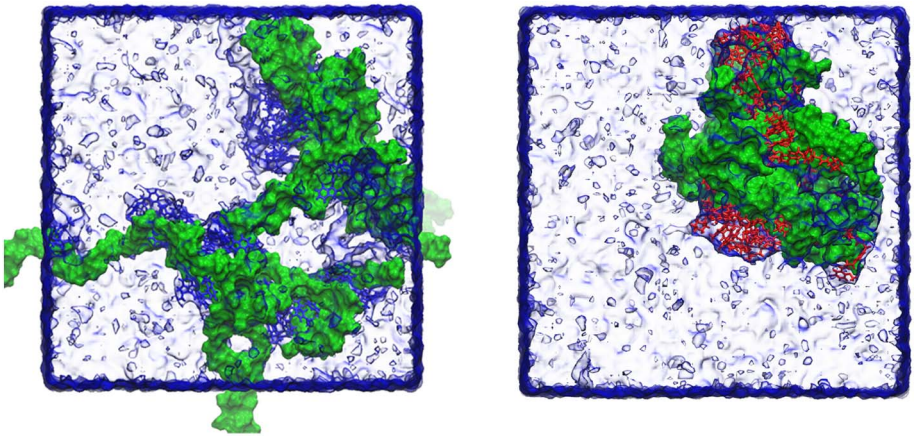

Fig. 6. Snapshots of the final frame (at 100 ns) for the molecular dynamics simulations of indapamide (left) and glibenclamide (right) and HPMC at the low number of molecules. Indapamide molecules are indicated in blue, glibenclamide in red and HPMC in green, with surrounding water molecules rendered as a transparent surface. During the course of the simulations, individual drug molecules associate and disassociate from the polymer chains in both cases. (For interpretation of the references to colour in this figure legend, the reader is referred to the web version of this article.)

3.4. Molecular dynamics (MD) simulations

A series of MD simulations were run to provide a better understanding of the molecular interactions between two of the model drugs (indapamide and glibenclamide) and the stabilizing polymer (HPMC) in supersaturated systems during dissolution. Indapamide and glibenclamide were selected as the model drugs based on the different dissolution profiles obtained experimentally in the presence of HPMC. Example snapshots of both indapamide and glibenclamide interacting with HPMC are shown in Fig. 6.

For these simulations we specifically analyzed the hydrogen bonding capacity. Fig. 7 shows the hydrogen bonds formed between individual drug molecules (either indapamide or glibenclamide) themselves, as well as between the drugs and HPMC. Each molecule of indapamide forms about 0.9 hydrogen bonds with other indapamide molecules, whereas glibenclamide forms roughly 0.6 hydrogen bonds with other glibenclamide molecules (see Fig. 7). In this case, there are many more indapamide (851) than glibenclamide (41) molecules in roughly the same volume (see Table 2). Therefore, for a simple probabilistic reason this result is expected but at a first glance it indicates that indapamide has a higher tendency to aggregate through formation of hydrogen bonds which is a driving force for crystallization.

When equal number of molecules is used instead, this effect is not observed (see Fig. 7). Instead, in these simulations it is observed that there are fewer hydrogen bonds between indapamide molecules than between glibenclamide molecules. This is true both for systems with the same number of drug molecules as the number of indapamide (high number) and when using the number of glibenclamide molecules (low number) (see Fig. 7). The per-molecule drug–drug hydrogen bond number is lower for indapamide at both high and low numbers of molecules in the simulations (0.9 and 0.3, respectively) than for glibenclamide (1.0 and 0.6), with bootstrap resampling of the mean number of hydrogen bonds providing that these numbers are statistically different for indapamide and glibenclamide. On the other hand, indapamide forms more hydrogen bonds with the HPMC. A comparison of the simulated systems, with and without the HPMC, shows that the addition of HPMC affects the number of indapamide drug–drug hydrogen bonds (0.9 vs. 1.0) more than it does for glibenclamide, which forms similar number of drug–drug hydrogen bonds (see Fig. 7, Supplementary 5).

The hydrogen bond patterns between drug and water molecules were also analyzed. Each indapamide molecule forms 2.2 and 2.6 hydrogen bonds with water at high and low number of molecules, respectively. The corresponding number of drug–water hydrogen bonds

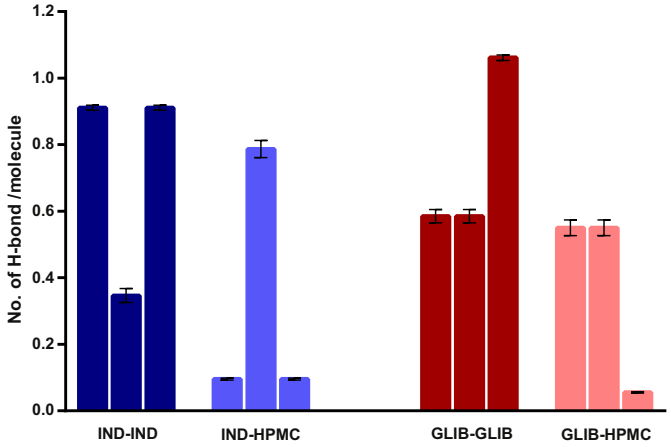

Fig. 7. Average number of hydrogen bonds (H-bond) per-molecule between individual indapamide molecules (IND–IND), indapamide molecules and HPMC (IND–HPMC), individual glibenclamide molecules (GLIB–GLIB) and glibenclamide molecules and HPMC (GLIB–HPMC) in three different systems with HPMC in the simulation box. Each bar in every dataset represents each system (from left to right) as follows: (i) unequal number of molecules; number of drug molecules corresponding to the 10-fold equilibrium solubility of indapamide (851) and glibenclamide (41), (ii) low number of molecules; number of molecules equal to the 10-fold equilibrium solubility of glibenclamide (41) for both indapamide and glibenclamide, and (iii) high number of molecules; number of molecules equal to the 10-fold equilibrium solubility of indapamide (851) for both indapamide and glibenclamide. The number of water molecules is fixed to 90% (w/w) in all systems. The error bars represent 95% confidence interval.

for glibenclamide is 1.7 and 2.3 (see Supplementary 6). Taken all together, these simulations suggest that indapamide satisfies a relatively larger part of its hydrogen bonding capacity either with HPMC or the surrounding water, whereas glibenclamide has more per-molecule drug-drug hydrogen bonds. The time evolution of these hydrogen-bond patterns are presented in the supplementary information (see Supplementary 5 and 6b).

4. Discussion

In this work we propose the application of a combined experimental approach to understand the initiation of crystallization in amorphous drugs during dissolution, with focus on spray-dried neat drugs and ASD. The methodology uses standard equipment found in pharmaceutical development laboratories and provides a robust, simple protocol, applicable on the small-scale, to identify the route(s) of crystallization during dissolution. This protocol for optimization of amorphous formulations may reduce drug development costs by reducing the chemicals, time and efforts needed to attain the same results as large-scale methods. More importantly, it may determine the suitability of amorphous formulation for a given drug, and allow the decision to be made at an early stage of the drug development. The step-wise approach is summarized in Fig. 2.

Before moving forward with the discussion, it is important to clarify that the approach undertaken in this study is to differentiate solid-to-solid and solution-mediated crystallization which may take place during dissolution of amorphous drug. A combination of DVS, DSC and PLM was used to investigate solid-to-solid crystallization whereas solution-mediated crystallization was studied by dissolution under non-sink conditions. Where necessary, other complementary methods were used. This included Raman spectroscopy which was used to study the polymorphism of glipizide and solvent-shift method to monitor the precipitation behaviour of glibenclamide to investigate if the decrease in concentration was due to pure solution-mediated crystallization and not due to particle-associated processes. This alludes to that for glibenclamide it could not be excluded that the surface of drug particles present in the dissolution medium promote nucleation of the supersaturated solution, which neither can be described as pure solid-to-solid mechanism nor a pure solution- mediated.

The initiation of crystallization within amorphous solid particles upon dissolution in water is mainly due to water sorption into the amorphous solid. This leads to increased molecular mobility which promotes nucleation and crystal growth. Similar water activity levels, as might occur upon water immersion, can be reached if the solid is exposed to water-saturated gas (100% RH). Under such experimental conditions, the water activity is similar in the solid, but the supersaturated solution is absent. Hence, the tendency seen for solid-to-solid crystallization, upon exposure of the amorphous solid to near 100% RH in the DVS (not 100% due to instrument limitations), presumably reflects the same tendency that the drugs show upon immersion in water during dissolution. Thus, exposure to 98% RH for 24 h in the DVS was used to mimic the condition during which amorphous solid particle get in contact with water in the beginning of dissolution process and used to identify drugs that show solid-state stability during the course of dissolution experiment.

The DSC and PLM were used to determine if the exposed drugs remained amorphous or crystallized. During a dissolution study, the high volume of water acts primarily as a solvent in which supersaturation occurs. The time during which a high level of supersaturation level can be maintained is limited, because as soon as the solution-mediated crystallization begins, the supersaturation level decreases [7,11]. It is important to emphasize that the combination of solid characterization methods used in this study were not meant to identify physical stability of amorphous drugs in their solid form upon storage, but rather used to identify solid-to-solid crystallization occurring during dissolution whereas the non-sink dissolution study was used to determine solution-mediated crystallization.

Based on the results, no solid-to-solid crystallization was shown with the solid-state characterization methods for three of the model drugs, (indapamide, metolazone and glibenclamide) after exposure to high humidity in the DVS chamber. This suggests that for these three amorphous drugs it is unlikely that solid-to-solid is the dominating mechanism of crystallization that results in unstable supersaturated system. Consequently, they do not necessarily need to be spray dried with any stabilizing polymer(s) as far as dissolution is concerned. Stabilizing polymer(s) might be necessary to maintain the physical stability, i.e. during processing, storage and handling, but the physical (dry) stability is outside the scope of this study.

The concentration-time profiles obtained from the dissolution studies proved that these three amorphous drugs precipitated mainly from supersaturated solution formed upon dissolution. The crystalline nature of the precipitates was confirmed with PLM. Low concentrations (0.001%–0.01% (w/v)) of HPMC were thereafter added to study if the polymer could prevent crystallization. These concentrations were selected as sufficiently high to inhibit crystallization but low enough not to affect the solubility of the amorphous drugs or to cause significant interactions with the surfaces of drug particles. At these concentrations, the crystallization of indapamide and metolazone was successfully blocked and minimized, respectively, during the course of dissolution studies. For both drugs, a higher level of supersaturation was achieved in the presence of HPMC, indicating that more amorphous solids were dissolved without the risk of crystallization and precipitation. Interestingly, PLM showed traces of crystallites in the metalazone samples, indicating that crystallization had initiated at a certain point during the dissolution study. However, the extent of crystallization was insufficient to drive precipitation of the crystals which ultimately results in decrease of drug concentration in the dissolution medium over time. From these measurements we conclude that the HPMC successfully blocked the crystallization of indapamide and reduced that of metolazone significantly.

In the absence of HPMC, glibenclamide displayed dissolution profiles similar to those of indapamide and metolazone. For glibenclamide, both HPMC concentrations reduced the crystallization rate and the HPMC also supported a higher level of supersaturation. Nevertheless, crystallization still occurred at both HPMC concentrations, as evidenced by the appearance of tiny crystals in the post-dissolution samples examined with PLM. The solvent shift method clarified that the glibenclamide was also precipitating when added from DMSO stock solution to the dissolution medium containing pre-dissolved HPMC, suggesting that the poor capacity of HPMC to maintain glibenclamide in solution was not due to particle-surface induced crystallization occurring at the particle–water surface. HPMC was only partly successful in blocking solution-mediated crystallization and maintaining supersaturation of glibenclamide to some extent; other polymers may be more useful for this particular drug.

In contrast, spray-dried neat glipizide exhibited high degree of crystallization after exposure to high humidity. This clearly indicates that transformation of amorphous glipizide — when exposed to water — will occur already in the solid amorphous particle. This is in agreement with previous studies on different model drugs including sulfadoxine, nifedipine and sucrose. For these compounds, crystallization starts on the surface of the amorphous solid and is propagated by the presence of water that acts as a plasticizer [12,31,32]. Coating the amorphous solid surface with a thin layer of polymer inhibits or delays this surface crystallization process. Thus, in this study, we attempted to spray dry ASD with glipizide and PVP (50:50% (w/w)) and then repeated the humidity condition. Apparently, the PVP in the ASD formulation did not completely stabilize the amorphous glipizide due to phase separation of the components in the ASD when it was exposed to water. The MDSC analysis of the post-DVS ASD essentially indicates a PVP-rich amorphous phase along with separate glipizide phase (see Supplementary 1). Additionally, a formation of small or

partially disordered glipizide crystals within the remaining amorphous PVP matrix may explain why crystalline phase was not observable in the PLM image of the post-DVS ASD samples (see Supplementary 2d). Collectively, this may also explain the higher dissolution rate and maximum concentration of glipizide from the ASD compared to the spray-dried neat glipizide (see Fig. 4d).

The DVS suggested that glipizide would undergo solid-to-solid transformation when exposed to water and this was confirmed in the dissolution studies of glipizide. Unlike the amorphous drugs discussed above, there was no spring-parachute dissolution pattern of glipizide, even in the $PhB_{6.5}$ with pre-dissolved HPMC. This suggests that amorphous glipizide immediately crystallized upon contact with $PhB_{6.5}$, so that only the dissolution profile of the crystallized glipizide was observed. Interestingly, the spray dried form had a higher apparent solubility than the unprocessed crystalline form. Based on the solid characterizations by DSC and PLM, glipizide was identified as undergoing crystallization via solid-to-solid pathway upon exposure to high humidity (discussed in Section 3.1). It was hypothesized that if solid-to-solid crystallization is the main crystallization pathway of glipizide upon immediate contact with water during dissolution, the dissolution behaviour of spray dried glipizide observed should be similar to that of the unprocessed crystalline glipizide if it crystallizes to the same polymorph. In our study, the concentration reached after 4 h with spray dried glipizide did not correspond to the unprocessed crystalline glipizide, suggesting that upon dissolution, it might have crystallized and transformed to another polymorph. The assumption that another glipizide polymorph was formed was further supported by analyzing peak positions in the Raman spectrum compared to the unprocessed crystalline glipizide. Previous work by Renuka and co-workers [33] report on a number of crystal forms existing for glipizide, but exact identification of polymorph formed in our dissolution studies was neither feasible nor within the scope of this paper.

A final question explored in this study was how and to what extent crystallization in supersaturated system is inhibited by the inclusion of polymer in the dissolution medium. To better understand the molecular interactions involved, MD simulations were performed on two of the model drugs (indapamide and glibenclamide). Experimentally, these had different dissolution behaviour and stabilization effects provided by the HPMC. To our knowledge, relatively few MD simulations have explored the underlying molecular interactions that govern drug-polymer interactions, especially during dissolution where high water content is present which makes the simulations relatively computer demanding. MD simulations can provide details of atomic-level structural and energetic factors that might explain the higher degree and longevity of stabilization of amorphous indapamide with HPMC compared to glibenclamide. One such molecular interaction is the hydrogen bond formation between the drug and polymer, which can inhibit crystallization. Our results showed that drug–drug and drug–-polymer hydrogen bonds affected the stability of amorphous formulations. The different stabilization effects of HPMC in the dissolution study may also have been an effect of the physicochemical properties of the model drugs, and hence the type and strength of interaction(s) involved. The influence of such properties on physical stabilization mechanism has been previously reported [34,35], and suggests that a larger, more systematic molecular dynamics study with more drugs and different polymers would be valuable to further test our hypothesis.

Our findings and approach improve the understanding of amorphous formulation design whereby unstable amorphous solid may recrystallize via either or both route(s) in solution. Identification and understanding of these crystallization routes may facilitate a rational choice of appropriate stabilizing strategies. The findings also imply that stabilization of different amorphous drugs cannot always be resolved using a single polymer. Different polymers or a combination of two or more polymers at different ratios may be required for optimum stabilization. The mechanism(s) of stabilization and/or destabilization by polymer inclusion in a given amorphous system may be predicted via MD simulations. By adopting this approach, one may then be able to identify if amorphous formulation is a suitable strategy to enable e.g. oral delivery of a given drug.

5. Conclusions

In this study, we successfully combined commonly used small-scale methods to provide insights into the crystallization pathways of amorphous drugs during dissolution. This strategy was also capable of identifying and rationalizing a mean to stabilize amorphous formulations from a dissolution perspective. Upon dissolution, amorphous drugs may basically crystallize via the solid-to-solid or the solution-mediated route — or in a worst case scenario — via both pathways. The four model drugs in this work reflected two pairs of analogues, for which the main difference in their dissolution performance was expected to be related to their solid-state properties. Indapamide and metolazone, both used in the treatment of cardiovascular disease, were stable in their amorphous form when exposed to water, and did not require formulation with polymers to maintain an amorphous solid material during dissolution. Once in solution, they became supersaturated and the crystallization was inhibited by low concentrations of HPMC. Glibenclamide and glipizide, two analogues used in the treatment of type II diabetes, had significantly different crystallization tendencies. Amorphous glibenclamide reached a supersaturated solution from which crystallization and precipitation occurred; this could not be fully blocked by the HPMC at the concentrations we used. On the other hand, glipizide suffered from solid-to solid crystallization which was partly inhibited by formulating the glipizide as an ASD with PVP K30. During dissolution of this ASD, glipizide crystallized and precipitated as a more soluble polymorph. The findings from our complementary MD simulations confirmed that hydrogen bond patterns between indapamide–HPMC and glibenclamide–HPMC are significantly different. The MD simulations point at that HPMC stabilizes indapamide better than glibenclamide through a higher number of hydrogen bonds formed, and this is likely an important mechanism for the better stabilization of the supersaturated indapamide solution.

Acknowledgements

The author, Khadijah Edueng is grateful for the financial support from Ministry of Higher Education and IIUM, Malaysia. This work has received support from the European Research Council Grant 638965 and the Swedish Research Council Grant 2014-3309. The molecular dynamics simulations were performed on resources provided by the Swedish National Infrastructure for Computing (SNIC) at the PDC Centre for High Performance Computing (PDC-HPC), the National Supercomputer Center (NSC) and the High Performance Computing Center North (HPC2N).

Appendix A. Supplementary data

Supplementary data to this article can be found online at http://dx.doi.org/10.1016/j.jconrel.2017.04.015.

References

[1] D. Horter, J.B. Dressman, Influence of physicochemical properties on dissolution of drugs in the gastrointestinal tract, Adv. Drug Deliv. Rev. 46 (2001) 75–87.
[2] D.D. Sun, P.I. Lee, Evolution of supersaturation of amorphous pharmaceuticals: nonlinear rate of supersaturation generation regulated by matrix diffusion, Mol. Pharm. 12 (2015) 1203–1215.
[3] S. Verma, V.S. Rudraraju, Wetting kinetics: an alternative approach towards understanding the enhanced dissolution rate for amorphous solid dispersion of a poorly soluble drug, AAPS Pharm. Sci. Technol. 16 (2015) 1079–1090.
[4] F. Tres, K. Treacher, J. Booth, L.P. Hughes, S.A. Wren, J.W. Aylott, J.C. Burley, Real time Raman imaging to understand dissolution performance of amorphous solid dispersions, J. Control. Release 188 (2014) 53–60.
[5] Y. Huang, W.G. Dai, Fundamental aspects of solid dispersion technology for poorly

soluble drugs, Acta Pharm. Sin. B 4 (2014) 18–25.
[6] M. Savolainen, K. Kogermann, A. Heinz, J. Aaltonen, L. Peltonen, C. Strachan, J. Yliruusi, Better understanding of dissolution behaviour of amorphous drugs by in situ solid-state analysis using Raman spectroscopy, Eur. J. Pharm. Biopharm. 71 (2009) 71–79.
[7] D.E. Alonzo, G.G. Zhang, D. Zhou, Y. Gao, L.S. Taylor, Understanding the behavior of amorphous pharmaceutical systems during dissolution, Pharm. Res. 27 (2010) 608–618.
[8] S. Ozaki, T. Minamisono, T. Yamashita, T. Kato, I. Kushida, Supersaturation-nucleation behavior of poorly soluble drugs and its impact on the oral absorption of drugs in thermodynamically high-energy forms, J. Pharm. Sci. 101 (2012) 214–222.
[9] S.B. Murdande, M.J. Pikal, R.M. Shanker, R.H. Bogner, Solubility advantage of amorphous pharmaceuticals: II. Application of quantitative thermodynamic relationships for prediction of solubility enhancement in structurally diverse insoluble pharmaceuticals, Pharm. Res. 27 (2010) 2704–2714.
[10] S. Ozaki, I. Kushida, T. Yamashita, T. Hasebe, O. Shirai, K. Kano, Evaluation of drug supersaturation by thermodynamic and kinetic approaches for the prediction of oral absorbability in amorphous pharmaceuticals, J. Pharm. Sci. 101 (2012) 4220–4230.
[11] S.A. Raina, D.E. Alonzo, G.G. Zhang, Y. Gao, L.S. Taylor, Impact of polymers on the crystallization and phase transition kinetics of amorphous nifedipine during dissolution in aqueous media, Mol. Pharm. 11 (2014) 3565–3576.
[12] M. Aucamp, M. Milne, W. Liebenberg, Amorphous sulfadoxine: a physical stability and crystallization kinetics study, AAPS Pharm. Sci. Technol. 17 (2016) 1100–1109.
[13] S. Ozaki, I. Kushida, T. Yamashita, T. Hasebe, O. Shirai, K. Kano, Inhibition of crystal nucleation and growth by water-soluble polymers and its impact on the supersaturation profiles of amorphous drugs, J. Pharm. Sci. 102 (2013) 2273–2281.
[14] D.E. Alonzo, Y. Gao, D. Zhou, H. Mo, G.G.Z. Zhang, L.S. Taylor, Dissolution and precipitation behavior of amorphous solid dispersions, J. Pharm. Sci. 100 (2011) 3316–3331.
[15] P.T. Mah, T. Laaksonen, T. Rades, L. Peltonen, C.J. Strachan, Differential scanning calorimetry predicts the critical quality attributes of amorphous glibenclamide, Eur. J. Pharm. Sci. 80 (2015) 74–81.
[16] D. Prasad, H. Chauhan, E. Atef, Amorphous stabilization and dissolution enhancement of amorphous ternary solid dispersions: combination of polymers showing drug-polymer interaction for synergistic effects, J. Pharm. Sci. 103 (2014) 3511–3523.
[17] U. Paaver, J. Heinamaki, I. Laidmae, A. Lust, J. Kozlova, E. Sillaste, K. Kirsimae, P. Veski, K. Kogermann, Electrospun nanofibers as a potential controlled-release solid dispersion system for poorly water-soluble drugs, Int. J. Pharm. 479 (2015) 252–260.
[18] A.L. Sarode, S.A. Malekar, C. Cote, D.R. Worthen, Hydroxypropyl cellulose stabilizes amorphous solid dispersions of the poorly water soluble drug felodipine, Carbohydr. Polym. 112 (2014) 512–519.
[19] S.B. Andersson, C. Alvebratt, J. Bevernage, D. Bonneau, C. da Costa Mathews, R. Dattani, K. Edueng, Y. He, R. Holm, C. Madsen, T. Muller, U. Muenster, A. Mullertz, K. Ojala, T. Rades, P. Sieger, C.A. Bergstrom, Interlaboratory validation of small-scale solubility and dissolution measurements of poorly water-soluble drugs, J. Pharm. Sci. 105 (2016) 2864–2872.
[20] J. Wang, R.M. Wolf, J.W. Caldwell, P.A. Kollman, D.A. Case, Development and testing of a general amber force field, J. Comput. Chem. 25 (2004) 1157–1174.
[21] S. Pronk, S. Pall, R. Schulz, P. Larsson, P. Bjelkmar, R. Apostolov, M.R. Shirts, J.C. Smith, P.M. Kasson, D. van der Spoel, B. Hess, E. Lindahl, GROMACS 4.5: a high-throughput and highly parallel open source molecular simulation toolkit, Bioinformatics 29 (2013) 845–854.
[22] M.J. Abraham, T. Murtola, R. Schulz, S. Páll, J.C. Smith, B. Hess, E. Lindahl, GROMACS: high performance molecular simulations through multi-level parallelism from laptops to supercomputers, Software X 1–2 (2015) 19–25.
[23] E. Vanquelef, S. Simon, G. Marquant, E. Garcia, G. Klimerak, J.C. Delepine, P. Cieplak, F.Y. Dupradeau, R.E.D. Server: a web service for deriving RESP and ESP charges and building force field libraries for new molecules and molecular fragments, Nucleic Acids Res. 39 (2011) W511–W517.
[24] M. Lundborg, E. Lindahl, Automatic GROMACS topology generation and comparisons of force fields for solvation free energy calculations, J. Phys. Chem. B 119 (2015) 810–823.
[25] L. Martínez, R. Andrade, E.G. Birgin, J.M. Martínez, PACKMOL: a package for building initial configurations for molecular dynamics simulations, J. Comput. Chem. 30 (2009) 2157–2164.
[26] G. Bussi, D. Donadio, M. Parrinello, Canonical sampling through velocity rescaling, J. Chem. Phys. 126 (2007) 014101.
[27] M. Parrinello, A. Rahman, Polymorphic transitions in single crystals: a new molecular dynamics method, J. Appl. Phys. 52 (1981) 7182–7190.
[28] T. Darden, D. York, L. Pedersen, Particle mesh Ewald: an N·log(N) method for Ewald sums in large systems, J. Chem. Phys. 98 (1993) 10089–10092.
[29] B. Hess, P-LINCS: a parallel linear constraint solver for molecular simulation, J. Chem. Theory Comput. 4 (2008) 116–122.
[30] W. Humphrey, A. Dalke, K. Schulten, VMD: visual molecular dynamics, J. Mol. Graph. 14 (1996) 33–38 (27-38).
[31] M. Mehta, K. Kothari, V. Ragoonanan, R. Suryanarayanan, Effect of water on molecular mobility and physical stability of amorphous pharmaceuticals, Mol. Pharm. 13 (2016) 1339–1346.
[32] X. Yu, S.M. Kappes, L.A. Bello-Perez, S.J. Schmidt, Investigating the moisture sorption behavior of amorphous sucrose using a dynamic humidity generating instrument, J. Food Sci. 73 (2008) E25–E35.
[33] Renuka, S.K. Singh, M. Gulati, I. Kaur, Characterization of solid state forms of glipizide, Powder Technol. 264 (2014) 365–376.
[34] M.B. Rask, M.M. Knopp, N.E. Olesen, R. Holm, T. Rades, Influence of PVP/VA copolymer composition on drug-polymer solubility, Eur. J. Pharm. Sci. 85 (2016) 10–17.
[35] J. Knapik, Z. Wojnarowska, K. Grzybowska, L. Tajber, H. Mesallati, K.J. Paluch, M. Paluch, Molecular dynamics and physical stability of amorphous nimesulide drug and its binary drug-polymer systems, Mol. Pharm. 13 (2016) 1937–1946.